NeuroImage 45 (2009) 215–223

Contents lists available at ScienceDirect

NeuroImage

journal homepage: www.elsevier.com/locate/ynimg

Multimodal imaging in mild cognitive impairment: Metabolism, morphometry and diffusion of the temporal–parietal memory network

K.B. Walhovd [a,b,*], A.M. Fjell [a,b], I. Amlien [a], R. Grambaite [c,d], V. Stenset [c,d], A. Bjørnerud [e,f], I. Reinvang [a], L. Gjerstad [g], T. Cappelen [h], P. Due-Tønnessen [e], T. Fladby [c,d]

[a] Center for the Study of Human Cognition, Department of Psychology, University of Oslo, Norway
[b] Ulleval University Hospital, Department of Neuropsychology, Norway
[c] Department of Neurology, Faculty Division, Akershus University Hospital, University of Oslo, Norway
[d] Department of Neurology, Akershus University Hospital, Lørenskog, Norway
[e] Department of Radiology, Rikshospitalet University Hospital, Oslo, Norway
[f] Department of Physics, University of Oslo, Norway
[g] Department of Neurology, Rikshospitalet University Hospital, Oslo, Norway
[h] Department of Nuclear Medicine, Rikshospitalet University Hospital, Oslo, Norway

ARTICLE INFO

Article history:
Received 16 June 2008
Revised 22 September 2008
Accepted 28 October 2008
Available online 13 November 2008

ABSTRACT

This study compared sensitivity of FDG-PET, MR morphometry, and diffusion tensor imaging (DTI) derived fractional anisotropy (FA) measures to diagnosis and memory function in mild cognitive impairment (MCI). Patients (n=44) and normal controls (NC, n=22) underwent FDG-PET and MRI scanning yielding measures of metabolism, morphometry and FA in nine temporal and parietal areas affected by Alzheimer's disease and involved in the episodic memory network. Patients also underwent memory testing (RAVLT). Logistic regression analysis yielded 100% diagnostic accuracy when all methods and ROIs were combined, but none of the variables then served as unique predictors. Within separate ROIs, diagnostic accuracy for the methods combined ranged from 65.6% (parahippocampal gyrus) to 73.4 (inferior parietal cortex). Morphometry predicted diagnostic group for most ROIs. PET and FA did not uniquely predict group, but a trend was seen for the precuneus metabolism. For the MCI group, stepwise regression analyses predicting memory scores were performed with the same methods and ROIs. Hippocampal volume and FA of the retrosplenial WM predicted learning, and hippocampal metabolism and parahippocampal cortical thickness predicted 5 minute recall. No variable predicted 30 minute recall independently of learning. In conclusion, higher diagnostic accuracy was achieved when multiple methods and ROIs were combined, but morphometry showed superior diagnostic sensitivity. Metabolism, morphometry and FA all uniquely explained memory performance, making a multimodal approach superior. Memory variation in MCI is likely related to conversion risk, and the results indicate potential for improved predictive power by the use of multimodal imaging.

© 2008 Elsevier Inc. All rights reserved.

Introduction

Mild cognitive impairment (MCI) is often considered a preclinical stage of Alzheimer's disease (AD), with an annual conversion rate to AD of 6–25% (Petersen et al., 2001). AD is characterized by a specific pattern of cerebral atrophy and hypometabolism (Mosconi et al., 2007). The alterations in MCI are especially targeted at temporal and parietal areas comprising the hippocampus, entorhinal, parahippocampal, retrosplenial, posterior cingulate, precuneus, supramarginal, inferior parietal and middle temporal cortex (Barnes et al., 2007; Baron et al., 2001; Chetelat et al., 2003; De Santi et al., 2001; Du et al., 2007; Fischl et al., 2002; Fjell et al., 2008; Frisoni et al., 2002; Herholz et al., 2002; Ishii et al., 2005; Karas et al., 2008). Several of these areas are integral parts of the episodic memory network, as shown by imaging and patient studies (Buckner, 2004; Scoville and Milner, 1957). The temporal lobe has rich projections to parietal regions, important for the representation of information being retrieved (Wagner et al., 2005). Hence, temporal and parietal brain changes are presumed to underlie much of the prominent and progressive memory loss detectable even in early stages of AD.

Changes in these brain areas in MCI can be captured by different methods, including structural MRI, yielding morphometric information (Mosconi et al., 2007), measurement of water diffusion by Diffusion Tensor Imaging — DTI (Chua et al., 2008), and metabolic positron emission tomography — PET with 2[18F]fluoro-2-deoxy-D-glucose (FDG) as the tracer (Mosconi et al., 2007). Different brain characteristics relevant for understanding memory and memory problems in MCI and AD may be captured by the different methods (Chetelat et al.,

* Corresponding author. University of Oslo, Institute of Psychology, POB 1094 Blindern, 0317 Oslo, Norway.
E-mail address: k.b.walhovd@psykologi.uio.no (K.B. Walhovd).

1053-8119/$ – see front matter © 2008 Elsevier Inc. All rights reserved.
doi:10.1016/j.neuroimage.2008.10.053

2003; De Santi et al., 2001; Ishii et al., 2005; Muller et al., 2005). It has been assumed that FDG-PET may detect early neocortical dysfunction before atrophy appears (De Santi et al., 2001), and diffusion imaging-derived parameters have been reported to have as good as or greater diagnostic utility than volume measures in MCI (Fellgiebel et al., 2006, 2005; Kantarci et al., 2005; Muller et al., 2007; Zhang et al., 2007). However, FDG-PET, MR morphometry and DTI have all proven to differentiate between NC, MCI, and AD (Mosconi et al., 2007). The goal of the present study is to determine to what extent the methods overlap or explain unique variance in comparison of MCI and normal controls, and in predicting memory function in MCI.

Three hypotheses were made: *H1) PET, MRI morphometry and DTI are moderately intercorrelated, and contribute to explain unique variance in diagnostic group and memory function.* This is based on previous literature reporting metabolic, morphometric and fractional anisotropy (FA; DTI) reductions to varying degrees in MCI (Ishii et al., 2005; Mosconi et al., 2007; Muller et al., 2007). *H2) PET and DTI have somewhat superior sensitivity compared to morphometry.* This has been indicated by a few recent studies (De Santi et al., 2001; Fellgiebel et al., 2006, 2005; Muller et al., 2007; Zhang et al., 2007). *H3) The strongest imaging–memory relationships are found for medial temporal lobe (MTL) areas, and relationships of intermediate strength are found for lateral temporal and parietal areas.* This is based on the crucial role of MTL in memory and atrophic changes in MCI and AD starting in MTL areas, then spreading to parietal areas (Edison et al., 2007; Karas et al., 2008; Mosconi et al., 2007; Petersen et al., 2000; Rossi et al., 2007; Walhovd et al., 2004).

Materials and methods

Sample

Patients aged 40–79 with MCI (Gauthier et al., 2006) established for at least 6 months attending a university-based clinic between September 2005 and December 2007 were assessed for inclusion, and all included gave informed consent. Patients with no or very mild ADL problems, symptoms lasting ≥6 months, Global Deterioration Scale score — GDS (Auer and Reisberg, 1997; Reisberg et al., 1988) from 2 to 3 as determined from a clinical interview and screening tests (Mini Mental Status Examination — MMSE (Folstein et al., 1975), STEP parameters 13–20 and fluency, interference, numeral–letter items from the I-flex (Royall et al., 1992; Wallin et al., 1996) and Cognistat (Kiernan et al., 1987)) were included. All patients had CDR=0.5, 8 patients had GDS=2 and the remaining GDS=3. One patient with GDS=3 had MMS=23, but had normal employment and was self-sufficient. Criteria for exclusion were established psychiatric disorder, cancer, drug abuse, solvent exposure or anoxic brain damage. The patients were scanned on either of two different magnetic resonance (MRI) scanner sites, with two different 1.5 T magnets (see MRI scanning and analyses). Healthy volunteers without deficits related to memory, emotionality and tempo, primarily spouses of participating patients, were included in the study as controls. Potential controls were interviewed by a clinician, and only controls with a GDS score of 1 were included. Data from a subsample, on thickness across the cortical mantle, hippocampal volume and memory in relation to CSF biomarkers have been reported elsewhere (Fjell et al., 2008). All participants, patients and controls, had FDG-PET scans from the same site (see FDG-PET scanning and analyses). All scans were manually inspected for accuracy of segmentations and coregistrations. Based on this inspection, one patient was excluded due to major stroke, and one was excluded based on suspected normal pressure hydrocephalus with enlarged ventricles. After application of these criteria, the *n* was 44 MCI patients (23 males/21 females, mean age 61.5 yrs, SD 8.1, range 43–77, MMSE (Folstein et al., 1975)=27.8, SD=1.7, range=23–30) and 22 controls (11 males/11 females, mean age 62.2 yrs, SD 8.0, range 46–75). For analyses involving temporal DTI, one patient was excluded due to missing temporal DTI data, and one was excluded from analyses involving entorhinal FA due to a lack of voxels left for analyses after ROI erosion (see below). Hence, for ROI by ROI group comparisons by logistic regressions and *T*-tests, $n=44$, for all methods and areas except temporal FA, while for logistic regression analysis involving all ROIs simultaneously, $n=42$. Memory data was also missing for one additional patient, so for the memory analysis (involving all ROIs), $n=41$. All values were standardized to the total sample of patients w/o missing values for the variable in question, i.e. no missing replacement was made. The slightly variable patient sample size ($n=41$–44) in analyses is regrettable, but unfortunately hard to avoid in a study involving this many measures. *n* or degrees of freedom are explicitly stated for each analysis to avoid misunderstandings regarding number of participants included. The project was approved by a committee for medical research ethics.

MRI scanning and analyses

MR scans were from two sites (site 1: 11 controls, 17 patients; site 2: 11 controls, 25 patients). Site 1: Siemens Symphony 1.5 T with a conventional quadrature head coil. Two 3D magnetization prepared gradient echo (MP-RAGE), T1-weighted sequences in succession (TR/TE/TI/FA=2730 ms/3.19 ms/1100 ms/15°, matrix=256×192), 128 sagittal slices, thickness=1.33 mm, in-plane resolution of 1.0 mm×1.33 mm. Site 2: Siemens Espree 1.5 T. One 3D MP-RAGE, T1-weighted sequence (TR/TE/TI/FA=2400/3.65/1000/8°, matrix=240×192), 160 sagittal slices, thickness=1.2 mm, in-plane resolution of 1 mm×1.2 mm. As described in another publication on a subsample from this study (Fjell et al., 2008), volumes of hippocampus, cortex, and the lateral ventricles were estimated for the 6 healthy controls who were scanned on both scanners and correlated across scanners. The Pearson coefficients were of 0.99, 0.90, and 0.999 (all $p<.05$), respectively. Also, a newly developed atlas normalization procedure was used, which has been shown to increase the robustness and accuracy of the segmentations across different scanners (Han and Fischl, 2007). Mean differences in cortical thickness were generally within±0.1 mm across the brain surface. This indicates that change of scanner did not introduce much bias in the data. The pulse sequences for DTI were: site 1: $b=700$; 12 directions repeated twice; 1 bo-value per slice, TR=4300 ms, TE=131 ms, number of axial slices: 19, slice thickness=5 mm (gap 1.5 mm), in-plane resolution: 1.8×1.8 mm^2, bandwidth: 955 Hz/pixel. Site 2: $b=750$; 12 directions repeated 5 times; 5 bo-values per slice, TR=6100 ms, TE=117 ms, number of slices: 30, slice thickness: 3 mm (gap 1.9 mm), in-plane resolution: 1.2×1.2 mm^2, bandwidth: 840 Hz/pixel.

MR segmentations were performed using FreeSurfer 4.0.1 (http://surfer.nmr.mgh.harvard.edu/). For hippocampal volume calculations, an automated, fully 3D whole-brain segmentation procedure was used (Fischl et al., 2002, 2004), where a probabilistic atlas is used and a Bayesian classification rule is applied to assign a neuroanatomical label to each voxel. The atlas consists of a manually-derived training set created by the Center for Morphometric Analysis (http://www.cma.mgh.harvard.edu/) from 40 other subjects across the age range, including individuals with AD. The segmentation uses three pieces of information to disambiguate labels: 1) the prior probability of a given tissue class occurring at a specific atlas location, 2) the likelihood of the image given that tissue class, and 3) the probability of the local spatial configuration of labels given the tissue class. This latter term represents a large number of constraints on the space of allowable segmentations, and prohibits label configurations that never occur in the training set (e.g. hippocampus is never anterior to amygdala). A newly developed atlas normalization procedure was used, which has been shown to increase the robustness and accuracy of the segmentations across scanner platforms (Han and Fischl, 2007). The present segmentation of the hippocampal formation

includes dentate gyrus, cornu ammonis (CA) fields, subiculum/parasubiculum and the fimbria (Makris et al., 1999).

The cortical surface was reconstructed to measure thickness at each surface location, or vertex, using a semi-automated approach described elsewhere (Dale et al., 1999; Dale and Sereno, 1993; Fischl and Dale, 2000; Fischl et al., 1999a,b; Salat et al., 2004). Thickness measurements were obtained by reconstructing representations of the gray/white matter boundary and the pial surface (Dale et al., 1999; Dale and Sereno, 1993) and then calculating the distance between those surfaces at each point across the cortical mantle. This method uses both intensity and continuity information from the entire three dimensional MR volume in segmentation and deformation procedures to produce representations of cortical thickness. The surface is created using spatial intensity gradients across tissue classes and is therefore not simply reliant on absolute signal intensity. The surface produced is not restricted to the voxel resolution of the original data and thus are capable of detecting submillimeter differences between groups (Fischl and Dale, 2000). The technique has been validated via histological (Rosas et al., 2002) as well as manual measurements (Kuperberg et al., 2003). The cortical surface then is parcellated according to procedures described by Fischl et al. (Fischl et al., 2004), including the presently selected ROIs. Each surface location, or vertex, is assigned a neuroanatomical label based on 1) the probability of each label at each location in a surface-based atlas space, based on a manually parcellated training set; 2) local curvature information; and 3) contextual information, encoding spatial neighborhood relationships between labels (conditional probability distributions derived from the manual training set). The parcellation scheme (Desikan et al., 2006) labels cortical sulci and gyri, and thickness values are calculated in the ROIs. The ROIs used here were extracted as described by Desikan et al. (2006). They defined 34 ROIs manually in each hemisphere in 40 scans. This information was then encoded in the form of an atlas that was used to automatically label ROIs. The automatically and the manually defined ROIs had an average intraclass correlation coefficient of 0.84, and a mean distance error of less than 1 mm. The same algorithm was used to define the ROIs in the present paper.

Based on the cortical parcellation, a newly developed algorithm was used to calculate WM labels in the gyrus underneath each cortical label. Each WM voxel within a gyrus was labeled according to the label of the nearest cortical voxel. Deep WM was not assigned to a particular cortical area, with a 5 mm distance limit. This yielded one WM area corresponding to each cortical area. The volume of each region was obtained by counting the number of 1 mm^3 voxels included (all scans were re-sampled to 1 mm isotropic voxels during the first FreeSurfer processing step), and these labels were used for calculation of WM FA. A three dimensional illustration of the segmentation of the ROIs used in the present article is shown in Fig. 1.

The preprocessing of the diffusion data involved motion and eddy-current correction. Each DW image was registered to the T2-weighted low-*b* (*b*=0) image (i.e. the image with no diffusion encoding). This registration is a 12 parameter affine one, and accounts for both motion between scans, and for residual eddy-current distortions present in the diffusion weighted images. Note that for the balanced echo sequences the eddy current distortions are small, and in our experience the 12 parameter transforms are sufficient to remove the remaining warping. A rigid transform was computed that maximizes the mutual information between the T1-weighted anatomical and the T2-weighted low-*b* image. General linear modeling was used to fit the tensors to the data and create the FA and tensor maps, in addition to three eigenvector and eigenvalue maps. The low-*b* volume was registered to each subject's anatomical volume, and the FA, eigenvector, and eigenvalue maps were analyzed in register with the low-*b*. Mean FA were calculated in each of the WM ROIx in each hemisphere (see Figs. 1 and 2). To avoid the problem of partial volume effects near the GM/WM border, each label was eroded by one voxel. Only FA values within the remaining WM area were used in the analyses. The probability of gray matter voxels being included was assumed to be extremely low. Since each participant's FA volume was only registered to the same participant's anatomical volume, the problem of spurious differences in FA due to imperfect inter-participant registration and gross anatomical differences was greatly reduced. This method has been validated by comparison with atlas based tractography, yielding almost identical FA values (Fjell et al., in press). One patient was excluded from analyses involving temporal FA, due to failure to localize DTI images correctly to selected temporal lobe ROIs (WM underlying entorhinal, parahippocampal, and middle temporal cortex). One patient was excluded from analyses involving entorhinal FA due to missing WM in the entorhinal cortex WM label in both hemispheres after erosion. For 3 patients and 1 control, entorhinal WM was left in only one hemisphere after erosion prior to extracting FA values. These subjects were not excluded from analyses, since average FA was used and since there was available WM after erosion for both hemispheres for all other ROIs.

FDG-PET scanning and analyses

18F-FDG PET/CT imaging was performed with a Biograph 16 PET/CT scanner (Siemens). Subjects fasted for at least 4 h prior to imaging (one patient had insulin-dependent diabetes and was allowed to have a light meal 2 h prior to scan). All patients and controls had FDG-PET scans, but a routine of measuring blood glucose on arrival was introduced after the study started, and therefore this was done for a subsample comprising 30 patients and 12 controls only. For these subjects, blood glucose was in the range 4.3–6.8 mmol/L,

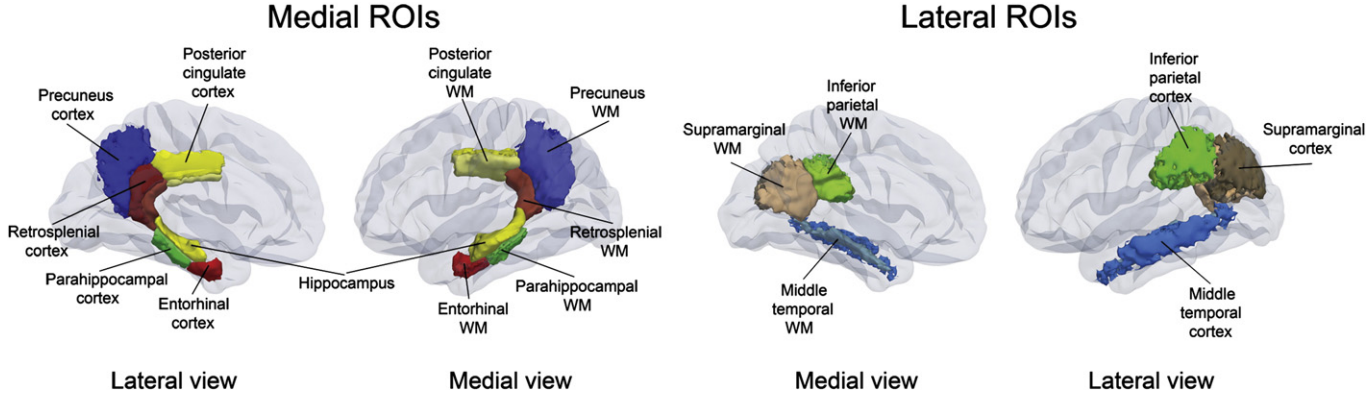

Fig. 1. 3D renderings of the hippocampus, cortical and white matter parcellations in an average brain made from the subjects scanned at site II. Both cortical and white matter parcellations are shown in the lateral and medial view, with white matter parcellations drawn in lighter colour nuances.

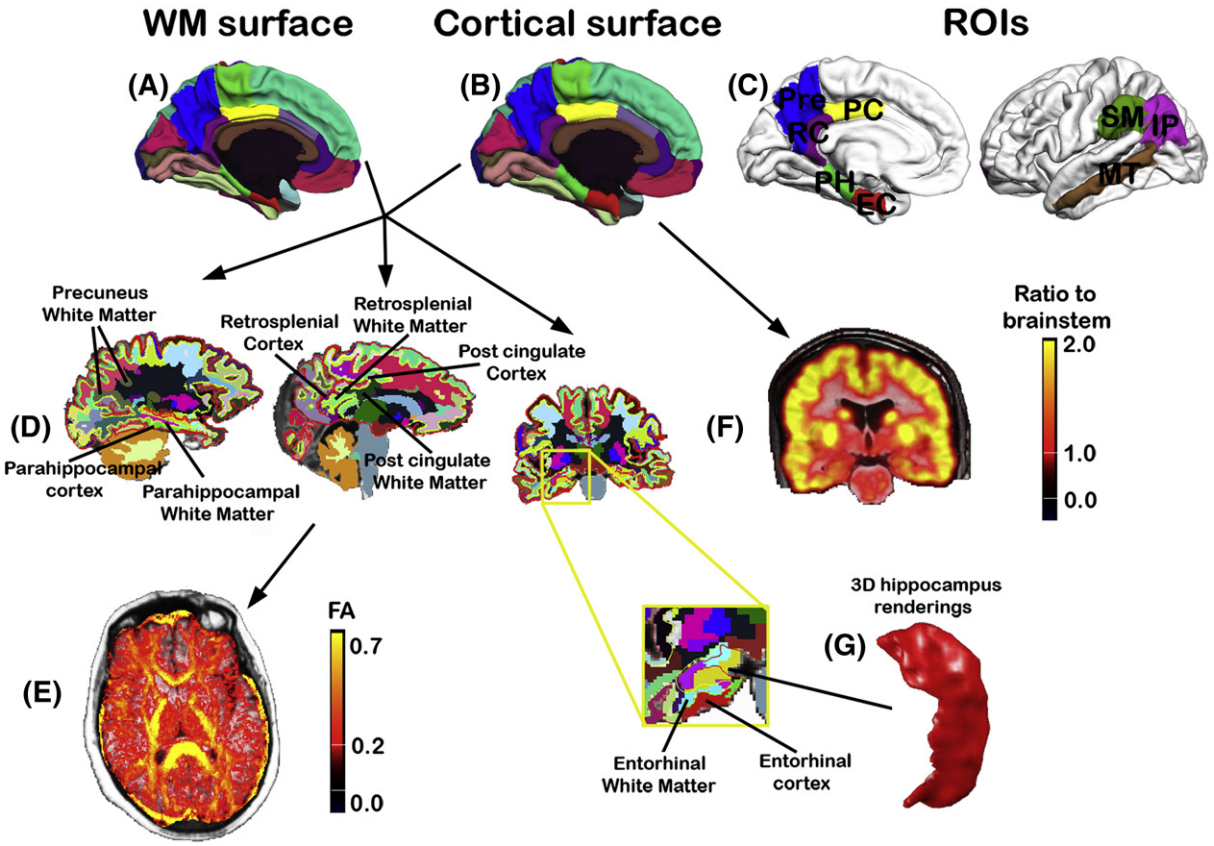

Fig. 2. The figure illustrates the main steps in the multi-modal image analysis. (A and B) The brain surface is parcellated into 34 different regions in each hemisphere (B), and a newly developed algorithm assigns a label to each underlying WM voxel (A). (C) Five cortical ROI's and hippocampus, of much importance in the episodic memory network, were chosen for analyses in the present paper. EC — entorhinal cortex; PH — parahippocampal cortex; RC — retrosplenial cortex; PC — posterior cingulate; Pre — precuneus. (D) Every voxel in each brain volume is assigned a label based on the cortical parcellations (A), the WM parcellations (B), and the whole-brain segmentation. The distance between the red and the yellow line is the cerebral cortex. (E) The FA volume is registered to the anatomical volume, and mean FA is calculated from the voxels included in each WM ROI (A). (F) FDG-PET data are also registered to the anatomical volume, and the metabolism is divided by the metabolism in the brainstem. Mean metabolism in each cortical ROI and hippocampus is calculated. (G) The whole-brain segmentation yields hippocampal volume (hippocampus is marked in yellow, indicated by the red arrows). A three-dimensional rendering of hippocampus is shown to illustrate the result of the segmentation.

except for the patient with insulin-dependent diabetes (11.0 mmol/L) and one control subject with diabetes type II (11.7 mmol/L). The images of these two subjects, as well as those of the subjects for whom blood glucose level at arrival was not registered, were deemed to be of satisfactory quality and hence, all were included in the analysis. Subjects had an intravenous bolus of 200 MBq 18F-FDG injected and rested for 45 min before scanning. A low-dose non-diagnostic CT scan was performed followed by a PET scan. The PET acquisition was performed in 3D mode with one single axial position, duration 15 min. Attenuation and scatter corrections were performed. The images were reconstructed by an iterative technique (5 iterations, 8 subsets), using a Gaussian smoothing filter with full width at half maximum (FWHM) of 3.5 mm. The image format was 256×256. For each subject, FDG-PET frames were registered to the corresponding intensity-normalized MRI volume. PET activity was averaged within each ROI defined on the MRI and normalized to activity within the brainstem. In order to correct for partial volume effects coupled with atrophy, volume (for the hippocampus) and cortical thickness (for the cortical ROIs) were regressed out of all PET variables, and the standardized residuals were used in most analyses (see below).

Regions of interest

ROIs were restricted to the hippocampus, entorhinal, parahippocampal, retrosplenial, posterior cingulate, precuneus, inferior parietal, supramarginal and middle temporal cortices, and the underlying WM (see Fig. 1), averaged across hemispheres. These ROIs were used to extract ROI PET and FA values (see Fig. 2). Intracranial volume (ICV) was calculated (Buckner et al., 2004) to control for differences in head size for hippocampal volumetric analyses.

Memory testing

RAVLT (Schmidt, 1996) was used to measure episodic memory in the patients. A list of 15 words is read aloud, and the patient subsequently recalls as many as possible. This is repeated five times with the same list of words, and the sum of words recalled across 5 trials yields a total learning score. Next, an interference list is read aloud and free recall is requested, before the patient is requested to recall the first list again without this being repeated (5 minute recall). After 30 min, the patient is asked to recall the first list of words with no re-reading (30 minute recall). The number of intrusions, i.e. falsely recalled items, was subtracted for the 5th learning trial, total learning, 5 minute and 30 minute recall scores (5th learning trial: M=9.1, SD=3.3, range=2–15; total learning: M=35.4, SD=12.1, range=11–66; 5 minute recall: M=6.3, SD=4.1, range=−2–15; 30 minute recall: M=6.1, SD=4.2, range=−1–14). These scores were standardized to the sample and used in the statistical analysis.

Statistical analyses

First, the different methods were correlated for each ROI, with age, gender and MR site controlled for. In this analysis, the PET variables were used without volume/thickness regressed out, since that would

per se make PET and MR uncorrelated, and the relationship between the two may be interesting from a clinical point of view. Next, the standardized residuals with effects of MR site (for morphometry/DTI), volume/thickness (for PET), age, and gender regressed out, were used in the group analyses. Logistic regression analysis was performed with 3 methods (metabolism, cortical thickness and FA of WM) for each of 8 ROIs (entorhinal, parahippocampal, retrosplenial, posterior cingulate, precuneus, supramarginal, inferior parietal and middle temporal cortices) with diagnostic group (MCI, NC) as the dependent variable. Then, to investigate the demographic and ROI variables' sensitivity to variance in memory function within the MCI group, stepwise regression analyses were performed with the following dependent variables in turn: 1) total learning, 2) 5 minute recall, and 3) 30 minute recall with the score on the last learning trial also entered among the predictors. Correlation analyses were also performed with the memory and ROI variables.

Results

Group comparisons and interrelations among methods

Group values for the different ROIs, standardized to sample w/ effects of age, gender, MR site (MR/DTI), and volume (PET) regressed out, are shown in Fig. 3. Intercorrelations of the different methods are shown in Table 1. The measures generally did not correlate strongly within ROIs. The logistic regression analyses with all 26 variables (9 MR+9 PET+8 FA) yielded a classification accuracy of 100%. No single variable then explained unique variance. The results of logistic regression analyses for each ROI separately with data from the different methods entered as predictor variables, are shown in Table 2. Diagnostic accuracy ranged from baseline probability (65.6%, due to unequal percentages of NC and MCI) for parahippocampal cortex to 73.6% for the inferior parietal cortex. For the parahippocampal ROI, no method was a significant predictor of diagnostic group, and for the posterior cingulate, GM thickness was marginally significant (p=.055). For all other ROIs, MR volumetry measures uniquely predicted diagnostic group. Metabolism was a marginally significant (p=.079) predictor besides GM thickness (p=.024) of the precuneus.

Table 1
Intercorrelations of the three methods for eight ROIs

	PET-GM thickness	PET-FA	GM thickness-FA
Entorhinal	**.42** (n=66)	.20 (n=64)	−.09 (n=64)
Parahippocampal	.27 (n=66)	.14 (n=65)	−.18 (n=65)
Retrosplenial	.26 (n=66)	−.02 (n=66)	−.06 (n=66)
Posterior cingulate	.05 (n=66)	**.31** (n=66)	−.12 (n=66)
Precuneus	.15 (n=66)	.07 (n=66)	−.02 (n=66)
Supramarginal	.23 (n=66)	.05 (n=66)	−.07 (n=66)
Inferior parietal	**.35** (n=66)	.22 (n=66)	−.02 (n=66)
Middle temporal	**.35** (n=66)	.20 (n=65)	−.00 (n=65)

Significant correlations (p<.05) corrected for 3 comparisons, are printed in bold. GM thickness=cortical thickness, FA=fractional anisotropy of the gyral white matter underlying the cortical area. For hippocampus, only PET and volume data were available, r=**.31** (n=66), p=.012.

Theoretically, even if not being a unique predictor, FA could still single-handedly predict diagnostic group, to the extent that the variance explained by FA could be overlapping with that of MR morphometry and PET. However, independent samples *T*-tests showed no significant (p<.05) or trends towards (p<.10) group differences in FA for any of the ROIs. To ensure that different scanners did not mask a possible FA group effect, *T*-tests were also done for the FA values for sites 1 and 2 separately. There were still no near-significant group differences (all p>.20). For the other methods, group differences or trends were found, showing lower metabolism, thinner cortex, and/or smaller neuroanatomical volumes in patients relative to controls. For metabolic measures, Levene's test showed significant differences in equality of variances across groups for some of the ROIs. This should be noted as a possible limitation when interpreting the data, but corrected values were then used when reporting *df*, *t* and *p*. A significant difference was found for precuneus metabolism (t [1, 63.829]=2.137, p=.036), with a trend for posterior cingulate metabolism (t [1,62.883]=1.904, p=.061). For PET variables not corrected for atrophy, significant differences were found for

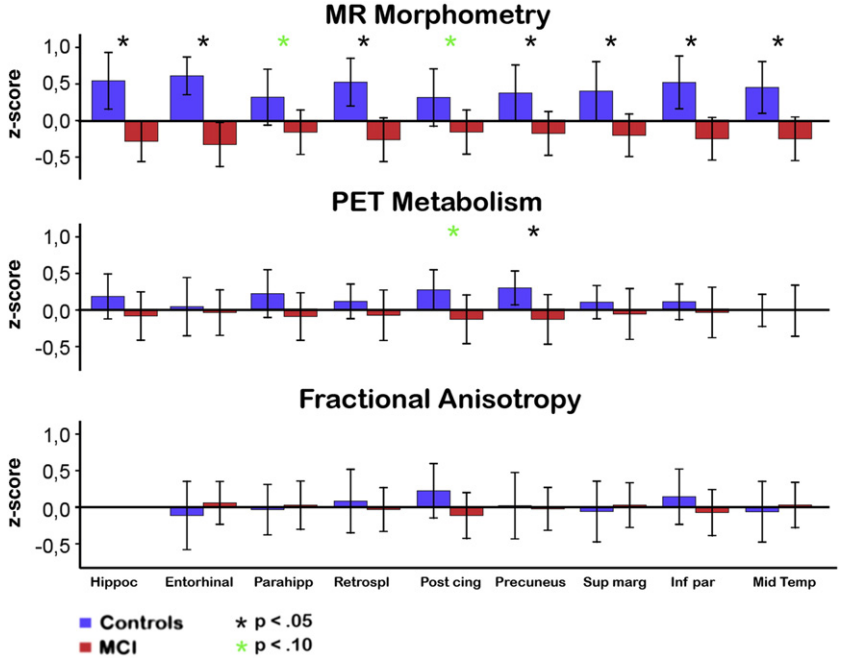

Fig. 3. Group values for the different ROIs, standardized to the total sample. The effects of age, gender, MR site for morphometry and DTI, and volume/thickness for PET, were regressed out, and the standardized residuals are depicted.

Table 2
Results from logistic regression analyses separately for each ROI

	Method	*B*	*p*	Odds ratio	% Correct classification	Nagelkerke *R* square
Hippocampus	PET	−.430	.160	.651	NC: 45.5	
n=66	MR volume	−1.168	.002	.311	MCI: 86.4	
					DA: 72.7	.261
Entorhinal cortex	PET	−.103	.761	.902	NC: 40.9	
n=64	GM thickness	−2.018	.001	.133	MCI: 81.0	
	FA	−.105	.747	.900	DA: 67.2	.363
Parahippocampal cortex	PET	−.362	.229	.693	NC: 18.2	
n=65	GM thickness	−.539	.076	.621	MCI: 93.0	
	FA	.050	.865	1.075	DA: 67.7	.101
Retrosplenial cortex	PET	−.303	.368	.738	NC: 36.4	
n=66	GM thickness	−1.058	.003	.347	MCI: 86.4	
	FA	−.264	.412	.768	DA: 69.7	.231
Posterior cingulate cortex	PET	−.396	.223	.673	NC: 36.4	
n=66	GM thickness	−.667	.043	.513	MCI: 90.9	
	FA	−.380	.235	.684	DA: 72.7	.159
Precuneus cortex	PET	−.615	.069	.540	NC: 31.8	
n=66	GM thickness	−.734	.027	.480	MCI: 90.9	
	FA	.010	.972	.990	DA: 71.2	.133
Supramarginal cortex	PET	−.241	.447	.786	NC: 27.3	
n=66	GM thickness	−.730	.022	.482	MCI: 90.9	
	FA	.054	.848	1.056	DA: 70.3	.117
Inferior parietal cortex	PET	−.291	.403	.748	NC: 40.09	
n=66						
	GM thickness	−1.077	.005	.341	MCI: 93.2	.209
Middle temporal cortex	PET	−.076	.821	.927	NC: 36.4	
n=66	GM thickness	−1.102	.007	.332	MCI: 90.7	
	FA	.110	.716	1.116	DA: 72.3	.195

hippocampal (t [1,63.167]=2.457, p=.017) and precuneus (t[1,63.999]=2.473, p=.016) metabolism, with trends for entorhinal (t[1,64]=1.910, p=.061), parahippocampal (t[1,64]=1.684, p=.097), retrosplenial (t[1,63.779]=1.841, p=.070), posterior cingulate (t [1,62.829]=1.928, p=.058), and inferior parietal (t [1,63.871]=1.993, p=.051) metabolism. For gray matter morphometry, significant group differences were found for hippocampal volume (t [1,64]=3.518, p=.001), and thickness of the entorhinal (t [1,64]=4.107, p=.000), retrosplenial (t [1,64]=3.316, p=.002), precuneus (t [1,64]=2.230, p=.029), supramarginal (t [1,64]=2.461, p=.017), inferior parietal (t [1,64]=3.234, p=.002), and middle temporal (t [1,64]=2.909, p=.005) cortices, with trends towards differences in thickness of the parahippocampal (t [1,64]=1.918, p=.060) and posterior cingulate (t [1,64]=1.890, p=.063) cortices.

Relationships of ROI imaging measures with neuropsychological memory function in MCI

Results of the stepwise regression analyses with total learning and 5 minute recall scores respectively, and the FDG-PET, DTI and MR volumetry variables, are shown in Table 3. Hippocampal volume and retrosplenial FA served as unique predictors of total learning, and together, these variables explained 37% of the variance in learning. Hippocampal metabolism and parahippocampal thickness served as unique predictors of 5 minute recall, and together, these variables explained 28% of the variance. The analysis with 30 minute recall as the dependent variable and the ROI variables, along with recall score at the 5th learning trial showed that only recall score at the 5th learning trial was then a unique predictor (F[1,39]=71.863, p=.000), explaining 37% of the variance. The regression plots for each of the ROI measures uniquely predicting a) total learning, and b) 5 minute recall, are shown in Fig. 4. Correlations for each ROI variable and these

Table 3
Stepwise regression analyses (n=41) with a) total learning score (standardized aggregate of hits minus intrusions for 5 learning trials) and b) 5 minute recall (standardized hits minus intrusion score) as the dependent variables

Total learning	β	p	R^2	F	Model p
Model 1					
Hippocampal volume	.46	.003	.21	10.338	.003
Model II					
Hippocampal volume	.58	.000			
Retrosplenial FA	.42	.004	.37	11.142	.000
5 minute recall					
Model I					
Hippocampal metabolism	.42	.007	.18	8.268	.007
Model II					
Hippocampal metabolism	.36	.013			
Parahippocampal thickness	.33	.021	.28	7.515	.002

measures are shown in Fig. 5. In general, the highest memory-morphometry correlations were found in the medial temporal ROIs. PET also showed temporal correlations, but tended to show stronger parietal learning correlations than morphometry. A dissociation between metabolism and morphometry was especially seen in the posterior cingulate, where thickness did not correlate, or correlated weakly and negatively with memory performance, while metabolism was significantly positively correlated with both learning and 5 minute

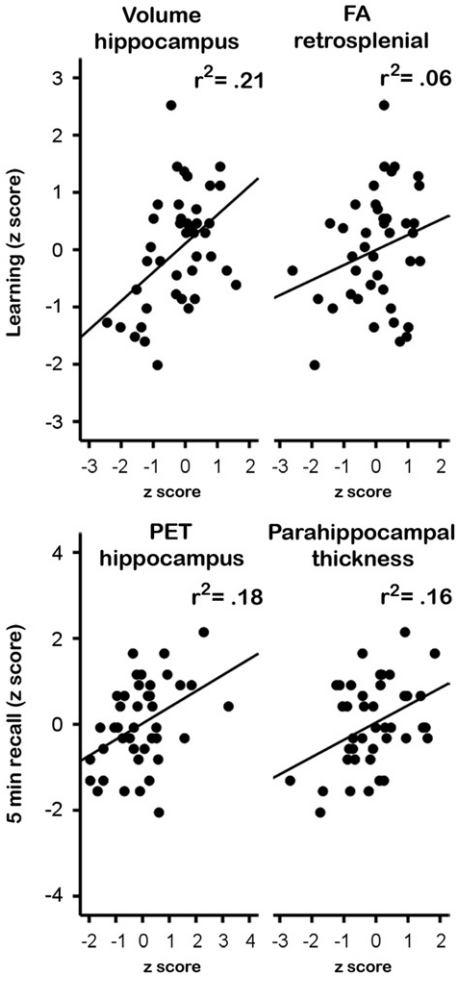

Fig. 4. Scatterplots depicting the relationship among a) total learning score and b) 5 minute recall and the ROI measures shown in stepwise regression analysis to explain unique variance in these memory measures. All plots show memory scores on the *Y*-axis, and values are standardized.

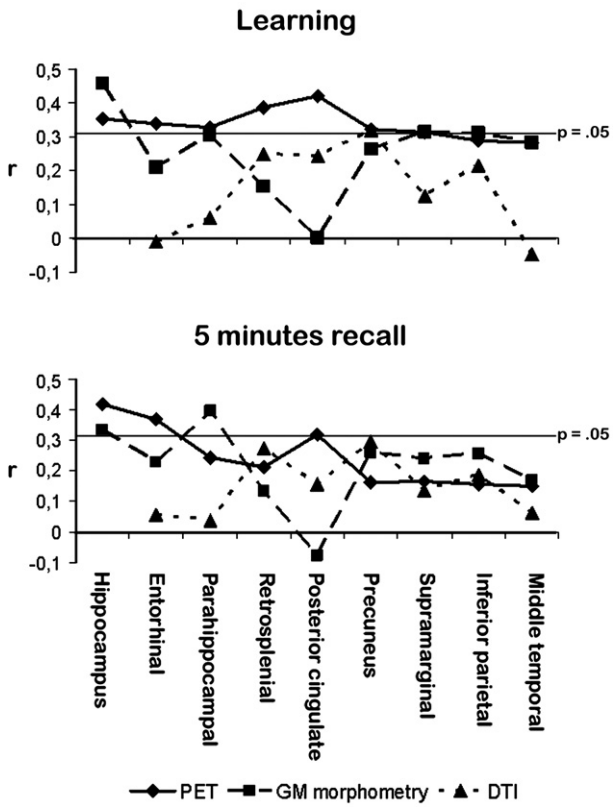

Fig. 5. Correlations between the different methodological measures from the 9 temporal and parietal ROIs and learning (upper panel) and 5 minute recall (lower panel). ROI measures were controlled for age and sex, as well as MR site for morphometry and DTI, and volume/thickness for PET. The dashed reference lines indicate $p = .05$.

recall. FA correlated only in the precuneus, where a significant positive relationship was seen for learning, and a trend towards the same for 5 minute recall.

Discussion

Incipient Alzheimer's disease may affect patients decades before the development of dementia, but diagnostic criteria and relevant biomarkers have not been established for this stage of the disease. Using multi-modal imaging, we aimed to determine which functional and structural parameters best identify patients versus controls at this stage, and explain the loss of memory in these patients. Three hypotheses were made based on earlier imaging findings and knowledge of the episodic memory network: 1) PET, MRI morphometry and DTI are moderately intercorrelated, and contribute to explain unique variance in diagnostic group and memory function. 2) PET and DTI have somewhat superior sensitivity compared to morphometry. 3) The strongest imaging–memory relationships are found for medial temporal lobe (MTL) areas, and relationships of intermediate strength are found for lateral temporal and parietal areas. Using logistic regression analyses, we found that 100% diagnostic accuracy could be achieved by entering imaging data obtained from nine temporal and parietal ROIs by three imaging modalities; PET, structural MRI, and DTI. Further analyses showed that morphometry best distinguished the diagnostic groups, but all imaging modalities explained unique variance in memory function. Hippocampal volume and retrosplenial FA explained learning, whereas hippocampal metabolism and thickness of the parahippocampal cortices best explained 5 minute recall. The data are further discussed in relation to the hypotheses below.

H1. PET, MRI morphometry and DTI are moderately intercorrelated, and contribute to explain unique variance in diagnostic group and memory function.

The correlations among methods within ROIs were surprisingly low. Correlations were found for PET and MR measures in the hippocampus and entorhinal, middle temporal and inferior parietal ROIs. However, FA was not related to MR morphometry in any ROI, and related to metabolism in the posterior cingulate only. Since both metabolic, morphometric and FA reductions have been reported in MCI (Ishii et al., 2005; Mosconi et al., 2007; Muller et al., 2007), one might expect some interrelations among the measures. A Pearson correlation of −.47 between hippocampal volume and apparent diffusion coefficient (ADC) in MCI has previously been reported in a diffusion weighted imaging (DWI) study (Kantarci et al., 2005). Still, the present findings for FA and MR are in line with another recent report, where normalized hippocampal volume and FA were not significantly related in MCI (Muller et al., 2007). However, both these studies employed diffusion measures (FA, mean diffusivity (MD) and ADC) taken within the hippocampus, a predominantly gray matter structure. These DTI measures are likely to reflect something different than FA within white matter ROIs such as used here, e.g. microscopic gray matter atrophy versus e.g. demyelination and axonal damage.

When entering all morphometry, metabolism and FA variables for all nine ROIs simultaneously, 100% diagnostic accuracy was achieved, which gives hope that multimodal imaging can indeed be clinically useful. However, only MR morhometry uniquely predicted diagnostic group when PET, MR morphometry and FA were entered simultaneously in logistic regression per ROI. Theoretically, even if not being unique predictors, metabolism and FA could still single-handedly predict diagnostic group, to the extent that the variance explained by these methods were overlapping with that of the others. This was in part the case for metabolism, for which a significant group difference was found in the precuneus, and a trend towards difference was seen in posterior cingulate metabolism. The present metabolism measures entered in group analyses were corrected for atrophy by removing, for each ROI, all variance associated with volume or thickness. This was done because tracer concentration measurement in small structures, e.g. cortical ROIs, can be confounded by limited spatial resolution (Samuraki et al., 2007), especially in atrophic brains, as might be the case in MCI patients. Signal changes due to atrophy is reflected both in the volumetric and original metabolic images, and potentially contribute to the sensitivity and predictive power of the methods. Partialing out variance from PET measures associated with atrophy may be seen as a strict, but probably correct approach, since non-existent tissue does not use metabolites and the volumetric images clearly most accurately reflect brain atrophy.

Brain atrophy may interact with metabolism in complex ways. It has been assumed that FDG-PET may detect early neocortical dysfunction before atrophy appears, and in one study, metabolism reductions were found to exceed volume losses in MCI (De Santi et al., 2001). However, in another study of cognitively impaired but not demented elderly, both cingulate hypometabolism and hippocampal atrophy were significant risk factors, but the latter was statistically more robust (Jagust et al., 2002; Wu et al., 2002). Ishii et al. (2005) also reported complementary diagnostic sensitivity of PET and MR in mild AD, with volumetric reductions in the MTL and metabolic reductions in the PC and parietal areas. It has been suggested that a metabolic/structural discrepancy in MTL could be a plastic response in mild AD, where early regional synaptic malfunction in affected areas cannot be detected due to compensatory activity in unaffected neurons (Geddes et al., 1985; Ishii et al., 2005, 1998; Matsuda et al., 2002). Another recent study with many of the same methods and ROIs as the present, also found morphometric variables to be at least as predictive of memory in MCI and AD as metabolic variables (Walhovd et al., in press), but unique variance was explained by each method. In the present study, when variance associated with volume/thickness was

not removed from the PET variables, additional group differences and trend towards such did indeed emerge. I.e. these PET results were clinically sensitive in and of themselves. However, this explained variance was not unique to PET, with the possible exception of precuneus metabolism, which showed a trend besides precuneus cortical thickness. Further, metabolism did explain unique variance in recall. Hence, based on the present data, MR morphometry was superior in predicting diagnostic group, and PET and MR morphometry both explained unique variance in memory.

FA was not a predictor of diagnostic group in the present study, and this did not appear due to variance overlapping with and explained by the other methods. However, group differences between MCI patients and controls in WM FA have previously been found (Fellgiebel et al., 2005; Zhang et al., 2007). Other differences may thus be influential. The present MCI group appears heterogeneous with respect to the wide range of RAVLT memory scores, but has on average relatively good memory scores. Their average MMSE score is higher than that of the MCI groups studied by Muller et al. (2007), and Fellgiebel et al. (2005), but comparable to that of the MCI group studied by Zhang et al. (2007).

The relatively weak inter-correlations among methods suggest that they may each explain unique variance. This was confirmed with regard to memory function. Hippocampal volume was the strongest unique ROI predictor in learning, explaining 21% of the variance. Adding retrosplenial FA yielded an increase in explained variance to 37%. Hippocampal metabolism explained 18% of the variance in 5 minute recall, and adding parahippocampal thickness increased the amount of explained variance to 28%. Brain variables did not add to the amount of explained variance in 30 minute recall when the last learning trial score was accounted for, and this may not be surprising given the relatively high amount of variance (37%) explained by the last learning trial score.

H2. PET and DTI have somewhat superior sensitivity compared to morphometry.

This was not supported for sensitivity to diagnostic classification. MR morphometry variables were the only unique predictors of diagnostic group when entered together with corresponding PET and DTI variables. For morphometry, group differences were found for seven of nine ROIs, with trends for the remaining two. For PET, a group difference was observed only for the precuneus, with a trend for the posterior cingulate cortices. When effects of volume or thickness were not removed from the PET variables, somewhat stronger results were observed, but still weaker than for GM morphometry: group differences were then observed for two of nine ROIs, and trends for five. The least predictive measure was FA, for which no group difference or trend towards such was observed in any ROI. This is in contrast to the recent studies by Muller et al. (2007) where superior diagnostic utility was found for hippocampal FA relative to hippocampal volume, and Zhang et al. (2007), where adding cingulum DTI to hippocampal volume improved diagnostic classification. Hippocampal diffusion measures have previously also been found to predict conversion from MCI to AD as well as or better than hippocampal volume (Fellgiebel et al., 2006; Kantarci et al., 2005). However, three of these studies (Fellgiebel et al., 2006; Kantarci et al., 2005; Muller et al., 2007) reported diffusion measures within hippocampal gray matter, rather than white matter structures within the MTL. All classes of measures demonstrated sensitivity to, and explained unique variance in memory performance. However, from the correlations depicted in Fig. 5, it is evident that PET and MR morphometry in general showed stronger memory relationships than FA measures.

H3. The strongest imaging–memory relationships are found for MTL areas, and relationships of intermediate strength are found for parietal areas.

This hypothesis was partly confirmed: the strongest memory relationships were found for the hippocampus for morphometry in learning and recall, and for PET in 5 minute recall. However, there was clearly also some dissociation across methods with regard to ROI sensitivity. For metabolism, memory relationships of comparable or higher strength than those found for MTL structures were found in parietal ROIs. This was especially true for the posterior cingulate, which showed significant positive metabolism correlations with learning and recall, whereas there was no (or even a slightly negative) relationship between memory performance and cortical thickness in this area. The predictive power of DTI in memory was greatest for the medial parietal structures, and there were no relationships or trends towards such between temporal FA and memory. Muller et al. (2005) have previously reported a positive relationship between hippocampal GM FA and verbal memory across MCI patients and controls. It is possible that the atrophic changes starting in MTL areas in MCI (Edison et al., 2007; Mosconi et al., 2007; Petersen et al., 2000; Rossi et al., 2007) have an effect on connected parietal white matter before gray matter change spreading to medial parietal areas can be detected. However, such effects were not visible in group comparisons. Rather, FA of the medial parietal areas may be especially important because of the rich interconnections of these structures with numerous other brain areas also playing part in memory (Buckner, 2004).

Conclusions and limitations

In conclusion: PET, MRI morphometry, and DTI were mostly weakly intercorrelated. Only morphometry explained unique variance in diagnostic group, but all methods explained unique variance in memory function. The present data did not support superior sensitivity of PET and DTI compared to morphometry, but did support superior sensitivity of a multi-modal approach to diagnosis and memory function. The strongest morphometry–memory relationships were found for medial temporal lobe (MTL) areas, while metabolism of the medial parietal areas were a least as much related to memory as metabolism of the medial temporal areas. This was especially true for learning. For DTI, only medial parietal memory relationships or trend towards such were seen. The present study has several limitations. The MCI group studied was included on the basis of clinical and functional criteria, but has a relatively broad range of memory scores, and may be heterogeneous also with respect to pathology. It remains to be seen what proportion will convert to AD, and to what extent the present neuroimaging findings can be related to differential pathology within the group. Neuropsychological data on controls should preferably be included in further studies, both to validate their memory function and to compare the memory–neuroimaging relationships identified in MCI-patients to such relationships in healthy persons. A further limitation is that MR scans from two sites were included. However, precautions were taken to ensure that this may not have influenced the results much. Individual differences in memory in MCI are likely related to conversion risk, and the results indicate potential for improved predictive power by use of multimodal imaging. The patients will be followed up to determine if and how multimodal imaging predicts cognitive decline and conversion to AD, and the sequence of changes in the different structures involved. It may be that the sensitivity of methods and their interrelations change as additional degenerative changes develop, and further studies are needed to clarify this.

References

Auer, S., Reisberg, B., 1997. The GDS/FAST staging system. Int. Psychogeriatr. 9 (Suppl. 1), 167–171.

Barnes, J., Scahill, R.I., Frost, C., Schott, J.M., Rossor, M.N., Fox, N.C., 2008. Increased hippocampal atrophy rates in AD over 6 months using serial MR imaging. Neurobiol. Aging. 29, 1199–1203.

Baron, J.C., Chetelat, G., Desgranges, B., Perchey, G., Landeau, B., de la Sayette, V., Eustache, F., 2001. In vivo mapping of gray matter loss with voxel-based morphometry in mild Alzheimer's disease. Neuroimage 14, 298–309.

Buckner, R.L., 2004. Memory and executive function in aging and AD: multiple factors that cause decline and reserve factors that compensate. Neuron 44, 195–208.
Buckner, R.L., Head, D., Parker, J., Fotenos, A.F., Marcus, D., Morris, J.C., Snyder, A.Z., 2004. A unified approach for morphometric and functional data analysis in young, old, and demented adults using automated atlas-based head size normalization: reliability and validation against manual measurement of total intracranial volume. Neuroimage 23, 724–738.
Chetelat, G., Desgranges, B., de la Sayette, V., Viader, F., Berkouk, K., Landeau, B., Lalevee, C., Le Doze, F., Dupuy, B., Hannequin, D., Baron, J.C., Eustache, F., 2003. Dissociating atrophy and hypometabolism impact on episodic memory in mild cognitive impairment. Brain 126, 1955–1967.
Chua, T.C., Wen, W., Slavin, M.J., Sachdev, P.S., 2008. Diffusion tensor imaging in mild cognitive impairment and Alzheimer's disease: a review. Curr. Opin. Neurol. 21, 83–92.
Dale, A.M., Sereno, M.I., 1993. Improved localization of cortical activity by combining EEG and MEG with MRI cortical surface reconstruction: a linear approach. Journal. of. Cognitive. Neuroscience. 5, 162–176.
Dale, A.M., Fischl, B., Sereno, M.I., 1999. Cortical surface-based analysis. I. Segmentation and surface reconstruction. Neuroimage 9, 179–194.
De Santi, S., de Leon, M.J., Rusinek, H., Convit, A., Tarshish, C.Y., Roche, A., Tsui, W.H., Kandil, E., Boppana, M., Daisley, K., Wang, G.J., Schlyer, D., Fowler, J., 2001. Hippocampal formation glucose metabolism and volume losses in MCI and AD. Neurobiol. Aging 22, 529–539.
Desikan, R.S., Segonne, F., Fischl, B., Quinn, B.T., Dickerson, B.C., Blacker, D., Buckner, R.L., Dale, A.M., Maguire, R.P., Hyman, B.T., Albert, M.S., Killiany, R.J., 2006. An automated labeling system for subdividing the human cerebral cortex on MRI scans into gyral based regions of interest. Neuroimage 31, 968–980.
Du, A.T., Schuff, N., Kramer, J.H., Rosen, H.J., Gorno-Tempini, M.L., Rankin, K., Miller, B.L., Weiner, M.W., 2007. Different regional patterns of cortical thinning in Alzheimer's disease and frontotemporal dementia. Brain 130, 1159–1166.
Edison, P., Archer, H.A., Hinz, R., Hammers, A., Pavese, N., Tai, Y.F., Hotton, G., Cutler, D., Fox, N., Kennedy, A., Rossor, M., Brooks, D.J., 2007. Amyloid, hypometabolism, and cognition in Alzheimer disease: an [11C]PIB and [18F]FDG PET study. Neurology 68, 501–508.
Fellgiebel, A., Muller, M.J., Wille, P., Dellani, P.R., Scheurich, A., Schmidt, L.G., Stoeter, P., 2005. Color-coded diffusion-tensor-imaging of posterior cingulate fiber tracts in mild cognitive impairment. Neurobiol. Aging 26, 1193–1198.
Fellgiebel, A., Dellani, P.R., Greverus, D., Scheurich, A., Stoeter, P., Muller, M.J., 2006. Predicting conversion to dementia in mild cognitive impairment by volumetric and diffusivity measurements of the hippocampus. Psychiatry. Res. 146, 283–287.
Fischl, B., Dale, A.M., 2000. Measuring the thickness of the human cerebral cortex from magnetic resonance images. Proc. Natl. Acad. Sci. U. S. A. 97, 11050–11055.
Fischl, B., Sereno, M.I., Dale, A.M., 1999a. Cortical surface-based analysis. II: inflation, flattening, and a surface-based coordinate system. Neuroimage 9, 195–207.
Fischl, B., Sereno, M.I., Tootell, R.B., Dale, A.M., 1999b. High-resolution intersubject averaging and a coordinate system for the cortical surface. Hum. Brain Mapp. 8, 272–284.
Fischl, B., Salat, D.H., Busa, E., Albert, M., Dieterich, M., Haselgrove, C., van der Kouwe, A., Killiany, R., Kennedy, D., Klaveness, S., Montillo, A., Makris, N., Rosen, B., Dale, A.M., 2002. Whole brain segmentation: automated labeling of neuroanatomical structures in the human brain. Neuron 33, 341–355.
Fischl, B., van der Kouwe, A., Destrieux, C., Halgren, E., Segonne, F., Salat, D.H., Busa, E., Seidman, L.J., Goldstein, J., Kennedy, D., Caviness, V., Makris, N., Rosen, B., Dale, A.M., 2004. Automatically parcellating the human cerebral cortex. Cereb. Cortex. 14, 11–22.
Fjell, A.M., Walhovd, K.B., Amlien, I., Bjørnerud, A., Reinvang, I., Gjerstad, L., Cappelen, T., Willoch, F., Due-Tønnessen, P., Grambaite, R., Skinningsrud, A., Stenset, V., Fladby, T., 2008. Morphometric changes in the episodic memory network and tau pathologic features correlate with memory performance in patients with mild cognitive impairment. Am. J. Neuroradiol. 29, 1–7.
Fjell, A.M., Westlye, L.T., Fischl, B., Due-Tonnessen, P., Bjørnerud, A., Greve, D., Benner, T., van der Kouwe, A.J.W., Salat, D., Walhovd, K.B., in press. The relationship between diffusion tensor imaging and volumetry as measures of white matter properties. Neuroimage.
Folstein, M.F., Folstein, S.E., McHugh, P.R., 1975. "Mini-mental state". A practical method for grading the cognitive state of patients for the clinician. J. Psychiatr. Res. 12, 189–198.
Frisoni, G.B., Testa, C., Zorzan, A., Sabattoli, F., Beltramello, A., Soininen, H., Laakso, M.P., 2002. Detection of grey matter loss in mild Alzheimer's disease with voxel based morphometry. J. Neurol. Neurosurg. Psychiatry 73, 657–664.
Gauthier, S., Reisberg, B., Zaudig, M., Petersen, R.C., Ritchie, K., Broich, K., Belleville, S., Brodaty, H., Bennett, D., Chertkow, H., Cummings, J.L., de Leon, M., Feldman, H., Ganguli, M., Hampel, H., Scheltens, P., Tierney, M.C., Whitehouse, P., Winblad, B., 2006. Mild cognitive impairment. Lancet 367, 1262–1270.
Geddes, J.W., Monaghan, D.T., Cotman, C.W., Lott, I.T., Kim, R.C., Chui, H.C., 1985. Plasticity of hippocampal circuitry in Alzheimer's disease. Science 230, 1179–1181.
Han, X., Fischl, B., 2007. Atlas renormalization for improved brain MR image segmentation across scanner platforms. IEEE Trans. Med. Imag. 26, 479–486.
Herholz, K., Salmon, E., Perani, D., Baron, J.C., Holthoff, V., Frolich, L., Schonknecht, P., Ito, K., Mielke, R., Kalbe, E., Zundorf, G., Delbeuck, X., Pelati, O., Anchisi, D., Fazio, F., Kerrouche, N., Desgranges, B., Eustache, F., Beuthien-Baumann, B., Menzel, C., Schroder, J., Kato, T., Arahata, Y., Henze, M., Heiss, W.D., 2002. Discrimination between Alzheimer dementia and controls by automated analysis of multicenter FDG PET. Neuroimage 17, 302–316.
Ishii, K., Sasaki, M., Yamaji, S., Sakamoto, S., Kitagaki, H., Mori, E., 1998. Relatively preserved hippocampal glucose metabolism in mild Alzheimer's disease. Dement. Geriatr. Cogn. Disord. 9, 317–322.
Ishii, K., Sasaki, H., Kono, A.K., Miyamoto, N., Fukuda, T., Mori, E., 2005. Comparison of gray matter and metabolic reduction in mild Alzheimer's disease using FDG-PET and voxel-based morphometric MR studies. Eur. J. Nucl. Med. Mol. Imaging 32, 959–963.
Jagust, W.J., Eberling, J.L., Wu, C.C., Finkbeiner, A., Mungas, D., Valk, P.E., Haan, M.N., 2002. Brain function and cognition in a community sample of elderly Latinos. Neurology 59, 378–383.
Kantarci, K., Petersen, R.C., Boeve, B.F., Knopman, D.S., Weigand, S.D., O'Brien, P.C., Shiung, M.M., Smith, G.E., Ivnik, R.J., Tangalos, E.G., Jack Jr., C.R., 2005. DWI predicts future progression to Alzheimer disease in amnestic mild cognitive impairment. Neurology 64, 902–904.
Karas, G., Sluimer, J., Goekoop, R., van der Flier, W., Rombouts, S.A., Vrenken, H., Scheltens, P., Fox, N., Barkhof, F., 2008. Amnestic mild cognitive impairment: structural MR imaging findings predictive of conversion to Alzheimer disease. AJNR Am. J. Neuroradiol. 29, 944–949.
Kiernan, R.J., Mueller, J., Langston, J.W., Van Dyke, C., 1987. The Neurobehavioral Cognitive Status Examination: a brief but quantitative approach to cognitive assessment. Ann. Intern. Med. 107, 481–485.
Kuperberg, G.R., Broome, M.R., McGuire, P.K., David, A.S., Eddy, M., Ozawa, F., Goff, D., West, W.C., Williams, S.C., van der Kouwe, A.J., Salat, D.H., Dale, A.M., Fischl, B., 2003. Regionally localized thinning of the cerebral cortex in schizophrenia. Arch. Gen. Psychiatry 60, 878–888.
Makris, N., Meyer, J.W., Bates, J.F., Yeterian, E.H., Kennedy, D.N., Caviness, V.S., 1999. MRI-Based topographic parcellation of human cerebral white matter and nuclei II. Rationale and applications with systematics of cerebral connectivity. Neuroimage 9, 18–45.
Matsuda, H., Kitayama, N., Ohnishi, T., Asada, T., Nakano, S., Sakamoto, S., Imabayashi, E., Katoh, A., 2002. Longitudinal evaluation of both morphologic and functional changes in the same individuals with Alzheimer's disease. J. Nucl. Med. 43, 304–311.
Mosconi, L., Brys, M., Glodzik-Sobanska, L., De Santi, S., Rusinek, H., de Leon, M.J., 2007. Early detection of Alzheimer's disease using neuroimaging. Exp. Gerontol. 42, 129–138.
Muller, M.J., Greverus, D., Dellani, P.R., Weibrich, C., Wille, P.R., Scheurich, A., Stoeter, P., Fellgiebel, A., 2005. Functional implications of hippocampal volume and diffusivity in mild cognitive impairment. Neuroimage 28, 1033–1042.
Muller, M.J., Greverus, D., Weibrich, C., Dellani, P.R., Scheurich, A., Stoeter, P., Fellgiebel, A., 2007. Diagnostic utility of hippocampal size and mean diffusivity in amnestic MCI. Neurobiol. Aging 28, 398–403.
Petersen, R.C., Jack Jr., C.R., Xu, Y.C., Waring, S.C., O'Brien, P.C., Smith, G.E., Ivnik, R.J., Tangalos, E.G., Boeve, B.F., Kokmen, E., 2000. Memory and MRI-based hippocampal volumes in aging and AD. Neurology 54, 581–587.
Petersen, R.C., Stevens, J.C., Ganguli, M., Tangalos, E.G., Cummings, J.L., DeKosky, S.T., 2001. Practice parameter: early detection of dementia: mild cognitive impairment (an evidence-based review). Report of the Quality Standards Subcommittee of the American Academy of Neurology. Neurology 56, 1133–1142.
Reisberg, B., Ferris, S.H., de Leon, M.J., Crook, T., 1988. Global Deterioration Scale (GDS). Psychopharmacol. Bull. 24, 661–663.
Rosas, H.D., Liu, A.K., Hersch, S., Glessner, M., Ferrante, R.J., Salat, D.H., van der Kouwe, A., Jenkins, B.G., Dale, A.M., Fischl, B., 2002. Regional and progressive thinning of the cortical ribbon in Huntington's disease. Neurology 58, 695–701.
Rossi, R., Geroldi, C., Bresciani, L., Testa, C., Binetti, G., Zanetti, O., Frisoni, G.B., 2007. Clinical and neuropsychological features associated with structural imaging patterns in patients with mild cognitive impairment. Dement. Geriatr. Cogn. Disord. 23, 175–183.
Royall, D.R., Mahurin, R.K., Gray, K.F., 1992. Bedside assessment of executive cognitive impairment: the executive interview. J. Am. Geriatr. Soc. 40, 1221–1226.
Salat, D.H., Buckner, R.L., Snyder, A.Z., Greve, D.N., Desikan, R.S., Busa, E., Morris, J.C., Dale, A.M., Fischl, B., 2004. Thinning of the cerebral cortex in aging. Cereb. Cortex 14, 721–730.
Samuraki, M., Matsunari, I., Chen, W.P., Yajima, K., Yanase, D., Fujikawa, A., Takeda, N., Nishimura, S., Matsuda, H., Yamada, M., 2007. Partial volume effect-corrected FDG PET and grey matter volume loss in patients with mild Alzheimer's disease. Eur. J. Nucl. Med. Mol. Imaging 34, 1658–1669.
Schmidt, M., 1996. Rey Auditory and Verbal Learning Test. Western Psychological Services, Los Angeles.
Scoville, W.B., Milner, B., 1957. Loss of recent memory after bilateral hippocampal lesions. J. Neurol. Neurosurg. Psychiatry 20, 11–21.
Wagner, A.D., Shannon, B.J., Kahn, I., Buckner, R.L., 2005. Parietal lobe contributions to episodic memory retrieval. Trends Cogn. Sci. 9, 445–453.
Walhovd, K.B., Fjell, A.M., Dale, A.M., McEvoy, L.K., Brewer, J., Karow, D.S., Salmon, D.P., Fennema-Notestine, C., Initiative, T.A.s.D.N., in press. Multi-modal imaging predicts memory performance in normal aging and cognitive decline. Neurobiol Aging
Walhovd, K.B., Fjell, A.M., Reinvang, I., Lundervold, A., Fischl, B., Quinn, B.T., Dale, A.M., 2004. Size does matter in the long run: hippocampal and cortical volume predict recall across weeks. Neurology 63, 1193–1197.
Wallin, A., Edman, A., Blennow, K., Gottfries, C.G., Karlsson, I., Regland, B., Sjogren, M., 1996. Stepwise comparative status analysis (STEP): a tool for identification of regional brain syndromes in dementia. J. Geriatr. Psychiatry Neurol. 9, 185–199.
Wu, C.C., Mungas, D., Petkov, C.I., Eberling, J.L., Zrelak, P.A., Buonocore, M.H., Brunberg, J.A., Haan, M.N., Jagust, W.J., 2002. Brain structure and cognition in a community sample of elderly Latinos. Neurology 59, 383–391.
Zhang, Y., Schuff, N., Jahng, G.H., Bayne, W., Mori, S., Schad, L., Mueller, S., Du, A.T., Kramer, J.H., Yaffe, K., Chui, H., Jagust, W.J., Miller, B.L., Weiner, M.W., 2007. Diffusion tensor imaging of cingulum fibers in mild cognitive impairment and Alzheimer disease. Neurology 68, 13–19.